World Scientific
www.worldscientific.com

JAPAN SOCIETY OF CIVIL ENGINEERS
COASTAL ENGINEERING COMMITTEE

Coastal Engineering Journal, Vol. 54, No. 2 (2012) 1250015 (25 pages)

DOI: 10.1142/S0578563412500155

TSUNAMI INUNDATION SIMULATION OF A BUILT-UP AREA USING EQUIVALENT RESISTANCE COEFFICIENT

JUNWOO CHOI

River, Coastal and Harbor Research Division,
Korea Institute of Construction Technology,
1190, Simindae-ro, Ilsan-gu, Goyang, Gyeonggi-do, 411-712, South Korea
jwchoi@kict.re.kr

KAB KEUN KWON

Department of Civil Engineering, Hanyang University,
17 Haengdang-dong, Seongdong-gu, Seoul, 133-791, South Korea
kkkwon@hanyang.ac.kr

SUNG BUM YOON*

Department of Civil and Environmental Engineering, Hanyang University,
1271 Sa3-dong, Sanrok-gu, Ansan, Gyeonggi-do, 426-791, South Korea
sbyoon@hanyang.ac.kr

Received 25 June 2010
Accepted 3 May 2012
Published 9 August 2012

An equivalent resistance coefficient that includes the effect of drag caused by buildings as well as the bottom friction effect was investigated for two-dimensional inundation simulation of built-up areas with relatively coarse grids. In order to quantify the equivalent resistance coefficient for a given built-up area, we performed laboratory experiments and three-dimensional numerical experiments of steady and uniform flows influenced by square unsubmerged piers spaced at equal intervals in the longitudinal and transverse directions. The Manning's n, which represents the equivalent resistance coefficient, was evaluated by

*Corresponding author.

inputting experimental data into the Manning's equation. A semi-analytical formula for the n value under experimental conditions was derived via momentum analysis that included drag interaction effects. The n values resulting from laboratory experimental data, the three-dimensional numerical data, and the semi-analytical formula agreed well with each other. From these results, we found that the equivalent resistance coefficient n value is strongly dependent on the intervals between piers and increases according to water depth to the 2/3 power. In addition, as an application of the proposed n formula to the inundation model, we performed a simulation of a tsunami inundation on Imwon Harbor on the east coast of Korea.

Keywords: Equivalent resistance coefficient; Manning's coefficient; inundation simulation; built-up area; drag interaction; laboratory experiment; three-dimensional numerical experiment; tsunami simulation; Imwon Harbor.

1. Introduction

In the last few decades, the incidence of ocean earthquakes, tsunamis, and flooding that affect coastal regions have increased. During urban floods, flow resistance caused by buildings increases the water surface elevation in built-up areas. To simulate coastal inundations over built-up areas, the shallow-water equations can be employed with a fine grid system implemented for resolving the buildings. In the fine grid system approach, the drag effect of the buildings is managed by the depth-averaged molecular and turbulent eddy viscous term. However, to simulate inundation in large built-up areas, the fine grid system requires impractical amounts of computational expense. As a practical alternative, coarse grid systems that omit the buildings can be used as long as the bottom friction term of the equation includes the effects of the drag resistance due to the buildings. For this approach, the coefficient of the bottom friction term, or the equivalent resistance (or roughness) coefficient (i.e. Manning's n [Chow, 1959]), must be quantified for a given built-up area.

Many studies have been carried out to investigate the equivalent resistance coefficient including the drag effects of emergent vegetation (such as mangrove trees) or plants in flooded areas. The experimental conditions in those studies vary in terms of flexibility, submergence, distributed density, size, and placement. Some previous studies involve flow resistance due to rigid and unsubmerged vegetation [Petryk and Bosmajian, 1975; Chiew and Tan, 1992; Naot *et al.*, 1996; Struve *et al.*, 2003; Musleh and Cruise, 2006; Yanagisawa *et al.*, 2009; Teh *et al.*, 2009]. Most of these investigations implemented the theory of flow resistance around a circular cylinder. However, there are few investigations of flow resistance caused by square unsubmerged buildings in flooded built-up areas [Aburaya and Imamura, 2002]. Naot *et al.* [1996] proposed a shading factor, which deals with the effects of drag interactions between vegetation elements only in the flow direction, but did not validate it. Most other previous investigations did not take into account hydraulic interactions between vegetation. Controversy persists over the relationship between the equivalent Manning's n and water depth in the flow on which unsubmerged rigid piers exert resistance. Musleh and Cruise [2006] showed that the n value increases

linearly with water depth, while other investigations suggested or implied that the n value depends on water depth to the power of 2/3.

In this study, in order to quantify the equivalent resistance coefficient for a given built-up area, we performed laboratory experiments and three-dimensional numerical experiments of turbulent flows influenced by square unsubmerged rigid piers spaced at equal intervals in the longitudinal and transverse directions. The three-dimensional numerical experiment utilized the RANS (Reynolds Averaged Navier–Stokes) equation model with a volume of fraction (VOF) model in FLOW-3D, a computational fluid dynamics code [Flow Science, Inc., 2000]. The Manning's n, which represents the equivalent resistance coefficient, was evaluated by inputting the experimental data into the Manning's equation. A semi-analytical formula for the equivalent resistance coefficient under experimental conditions was derived from momentum analysis including drag interaction effects. Note that even though the experimental flows are instantaneously fluctuating due to the influence of the piers, their spatially and temporally averaged motion was assumed to be locally steady and uniform. This implies that we employ the conventional assumption that the resistance coefficient, which was estimated under conditions of steady and uniform flow, can be utilized in unsteady and nonuniform simulations by incorporating the shallow-water equation.

During experiments, we focused on the effects of drag interaction between the piers, which were aligned in rows, and the relationship of the n value to water depth. The semi-analytical formula and the measured and computed experimental data were compared. The relationships between the n value and hydraulic characteristics (water depth, size of piers, and transverse and longitudinal intervals of piers) were assessed. Aburaya and Imamura [2002] mentioned that the drag effects depend on shapes and alignments of buildings and unsteadiness of the flow, and presented an experimental result including longitudinal drag interaction in a wave channel. The present study proposes a general formula taking into account transverse drag interaction as well as longitudinal drag interaction of square unsubmerged rigid piers spaced at equal intervals.

In addition, as an application of the semi-analytical n formula, we performed a simulation of inundation at Imwon Harbor due to the 1983 Tsunami that occurred in the East Sea (Sea of Japan), the most destructive tsunami in the history of Korea. For this simulation, we utilized a linear Boussinesq-type wave equation model with a dispersion-correction technique for deep water propagation [Yoon *et al.*, 2007] and a nonlinear shallow-water equation model [Lim *et al.*, 2008] incorporating a moving boundary technique [Yoon and Cho, 2001] for inundation.

For this study, which investigated the equivalent resistance coefficient incorporating drag effects as well as bottom friction effect in a region with square unsubmerged rigid piers aligned in rows, we integrated and analyzed the results reported partially in Choi *et al.* [2009a, b], Kwon *et al.* [2010], and Bae *et al.* [2010] along with new results.

2. Theory

In a fully developed open channel flow with resistant bodies (such as unsubmerged rigid piers) the total flow resistance can be expressed by bottom friction and form drags of the bodies if the friction and the drags act independently and the flow is steady and uniform under the large eddy mean flow-concept. The momentum equation of equilibrium can be written as:

$$\rho g A L \sin\theta - \tau_s P L - N F_d = 0\,, \tag{1}$$

where g is gravitational acceleration, A is the cross-sectional flow area with neglecting resistant bodies, $\sin\theta$ is the channel slope, which is equal to the energy slope S_f for uniform flow, $\tau_s \equiv F_s/PL$ is the bottom shear stress, and N is the number of identically-shaped resistant bodies. The frictional resistance (F_s) and the drag resistance (F_d) can be replaced by $F_s = C_f \rho V^2 PL/2$ and $F_d = C_D \rho V^2 A_p/2$, where C_f is the skin-friction coefficient, C_D is the drag coefficient, ρ is water density, V is the approach velocity averaged over the cross-section, P is the wetted perimeter, L is channel length, and A_p is the projected area of a resistant body. Note that Eq. (1) implies that we ignore a possible interaction effect between the friction and the drag and overestimation of the bottom friction due to the place in which the bodies situated. If the resistant bodies are longitudinally and transversely aligned, the number of bodies N can be divided into N_F in the longitudinal direction and N_T in the transverse direction, i.e. $N = N_T \times N_F$. From Eq. (1), the energy slope S_f can be written as:

$$S_f = \left(\frac{C_f}{R_h} + \frac{N_F C_D}{L}\,\frac{N_T A_P}{A}\right)\frac{V^2}{2g}\,, \tag{2}$$

where $R_h = A/P$ is the hydraulic radius. Assuming that the bodies are unsubmerged piers, substituting Eq. (2) into the Manning's equation (i.e. $n^2 = S_f R_h^{4/3}/V^2$), and using the relations such as $C_f = f/4$, $N_F/L = 1/(s+b)$, $r_0 = 1 - N_T A_p/A$, and $n_b = \sqrt{f h^{1/3}/8g}$, the equivalent resistance coefficient (n), which is the value of n including the drag effect exerted by the piers as well as the bottom friction, can be written as:

$$n = \sqrt{n_b^2 + C_D\,\frac{1-r_0}{1+s/b}\left(\frac{h}{b}\right)\left(\frac{h^{1/3}}{2g}\right)}\,, \tag{3}$$

where f is the friction factor, s is the interval space in the longitudinal direction, b is the width of piers in the flow direction, r_0 is the porosity with respect to the cross-sectional flow area, n_b is the Manning's roughness coefficient for the bottom of channel, and h is water depth ($R_h = h$ for a wide channel). As mentioned earlier, Eq. (3) requires the assumption that drags caused by piers act independently.

However, if the interval spaces between the piers are insufficient, changes in flow occur due to interaction with adjacent piers. In other words, the drag resistance

of a pier influences the approach velocities of backward adjacent piers and their drag resistances. The hydraulic interaction between the piers can be called as "drag interaction." Therefore, we introduce a drag interaction coefficient C_{DI} in order to consider the effect of the drag interaction. Using the drag interaction coefficient C_{DI}, Eq. (3) is rewritten as:

$$n = \sqrt{n_b^2 + C_{\mathrm{DI}} C_D \frac{1 - r_0}{1 + s/b} \left(\frac{h}{b}\right) \left(\frac{h^{1/3}}{2g}\right)} \,. \tag{4}$$

Intuitively, it can be said that the drag interaction coefficient C_{DI} is a function of various parameters related to shape, projected area, placement, intervals of resistant bodies, water depth, Reynolds number, bottom roughness, and so on. However, in this study, C_{DI} is assumed to be dependent only on the interval and size of the pier within the turbulent region, $\mathrm{Re} > O(10^4)$, in which the drag coefficient C_D is constant for a square pier. The Reynolds number can be defined as $\mathrm{Re} = Vb/\nu$, where ν is the kinematic viscosity. This assumption will be discussed later in the context of experimental results.

Since the interaction between piers aligned in the longitudinal direction (the mean flow direction) do not operate according to the same mechanism as the interaction in the transverse direction, the drag interaction coefficient C_{DI} is calculated as:

$$C_{\mathrm{DI}} = C_{\mathrm{DIT}} C_{\mathrm{DIF}} \,, \tag{5}$$

where C_{DIF} is the longitudinal drag interaction coefficient and C_{DIT} is the transverse drag interaction coefficient. The longitudinal drag interaction coefficient C_{DIF} was empirically estimated to be a function of s/b using previously published experimental data [Choi *et al.*, 2009a], and was written as:

$$C_{\mathrm{DIF}} = 1 - 0.95 \exp\left(-0.39 \left(\frac{s}{b}\right)^{1.8}\right) . \tag{6}$$

The analysis of previously published experimental data, which yielded an empirical Eq. (6) for the longitudinal drag interaction coefficient, will be discussed in detail later in this paper. The transverse drag interaction coefficient C_{DIT} can be estimated by employing the orifice energy loss coefficient, $\alpha_s = (1/r_0 C_c - 1)^2$, where C_c is the contraction coefficient, i.e. $C_c = 0.6 + 0.4 r_0^2$ [Mei, 1989], since the mechanism of resistance (or energy loss) due to an orifice is analogous to that of resistance due to a gap between piers aligned in the transverse direction. The orifice energy loss coefficient α_s and the contraction coefficient C_c are derived based on the assumption of a sharp orifice, but the gaps between piers are better described as thick orifices. Therefore, the previously published thick orifice energy loss coefficient α [Yoon *et al.*, 2006] was employed and the transverse drag interaction coefficient is written as:

$$C_{\mathrm{DIT}} = \frac{\alpha}{C_D(1 - r_0)} \quad \text{for} \quad r_0 < 0.643 \,, \tag{7}$$

where

$$\alpha = \left[0.6 + 0.4\exp\left(-\frac{2.5b}{w}\right)\right]\left(\frac{1}{r_0 C_c} - 1\right)^2, \tag{8}$$

where w represents the pier interval in the transverse direction. If the piers are square, α can be rewritten as a function of the porosity, i.e. $b/w = (1 - r_0)/r_0$. It should be noted that the transverse drag interaction coefficient C_{DIT} in Eq. (7) cannot be applied outside of the region where the orifice energy loss coefficient is applicable. In other words, if the transverse interval space of the piers becomes wide enough, the drag resistance of piers acts independently and C_{DIT} approaches 1.0. Thus, if the piers are square, Eq. (7) is available when $r_0 < 0.643$, so that C_{DIT} should be larger than 1.0, and

$$C_{\mathrm{DIT}} = 1.0 \quad \text{for} \quad r_0 > 0.643\,. \tag{9}$$

The equivalent resistance coefficient given by Eq. (4) can be slightly modified when the intervals between piers are equal ($s = w$) to each other in both longitudinal and transverse directions. It is rewritten as:

$$n = \sqrt{n_b^2 + C_{\mathrm{DI}} C_D (1 - R_0)\left(\frac{h}{b}\right)\left(\frac{h^{1/3}}{2g}\right)}\,, \tag{10}$$

where R_0 is the porosity in the horizontal plane, defined as the fraction of flow area excluding the area of piers in the total plane area and $R_0 = 1 - (b/(s + b))^2$. For the n formula, defined as a function of the plane porosity R_0, the drag interaction coefficient C_{DIF} in Eq. (6) and C_{DIT} in Eq. (7) can be evaluated as a function of R_0 by using the following relationships: $r_0 = 1 - \sqrt{1 - R_0}$ and $s/b = 1/\sqrt{1 - R_0} - 1$. In other words, the semi-analytical formula (10) can be evaluated if the roughness coefficient n_b, the plane porosity R_0, the width of the pier b, and the water depth h are known.

3. Laboratory Experiments

3.1. *Model setup*

Laboratory experiments were performed in order to investigate the effects of drag interactions between piers and the relationship between the n value and water depth. We aligned 11.4 cm-wide square piers in 12 m-long and 0.4 m-wide channels as shown in Fig. 1. The square, unsubmerged and rigid piers were aligned in one row ($r_0 = 0.715$) or two rows ($r_0 = 0.43$) at longitudinal intervals of $0 \sim 1.1$ m. The channel was tilted with a slope of $0.001 \sim 0.01$. The downstream weir of the channel was manipulated to create various (large eddy mean) uniform flows in the range of discharges of $0.002 \sim 0.007$ m^3/s. The uniform flows were confirmed by measuring three (time-averaged) water depths at up, middle, and downstream points. The discharges were directly measured through filling a 3.0 m^3 tank with water from

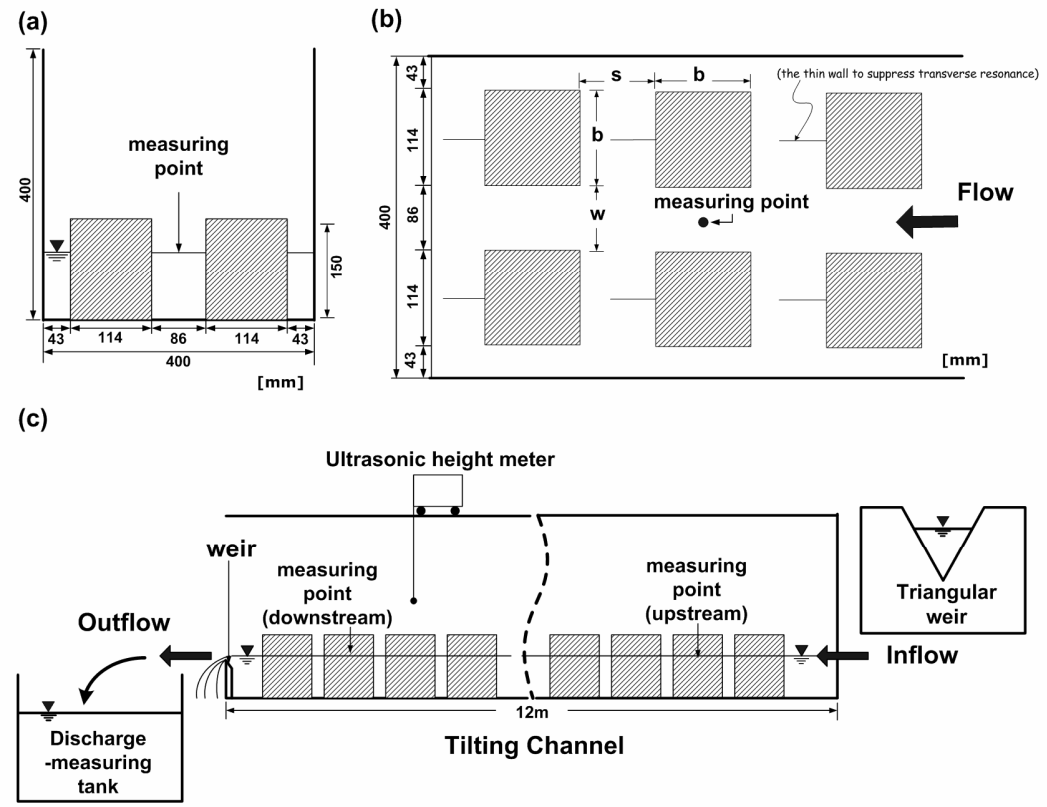

Fig. 1. Schematic diagrams of the laboratory experiment setup with two rows of square piers: (a) transverse sectional view, (b) plane view, and (c) longitudinal sectional view.

the outflow. The Manning's n, which is the equivalent resistance coefficient, was evaluated by substituting observed measurements of channel slope, water depth and discharge into the Manning's equation. The experiments were conducted in the turbulent region, Re $> O(10^4)$ to maintain a constant drag coefficient C_D for square piers. In order to suppress the transverse resonance of the free surface caused by vortex shedding, thin smooth walls were installed behind the piers along the longitudinal space (shown in Fig. 1(b)). The length of the thin smooth walls setup depending on the intervals of piers, the maximum length is the same as the pier's width, and the height is the same as the pier's height. Note that the effects of friction due to the side glass walls of the channel and the thin walls were neglected based on the assumption that when the drag resistance is dominant, the wall friction is negligible.

3.2. *Results*

The variations of the n values, as evaluated using measurements of channel slopes, water depths, and discharges, according to longitudinal intervals between the piers

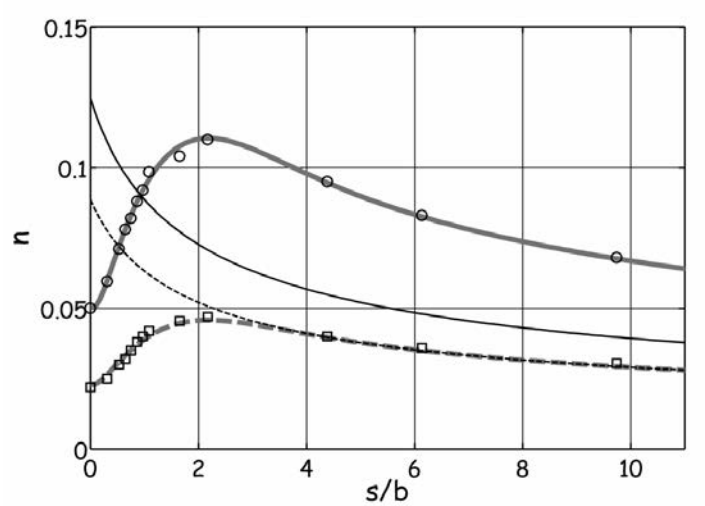

Fig. 2. Variation of the n values according to s/b when $h = 7$ cm. Laboratory data (□), analytical formula (3) (– – – –) and semi-analytical formula (4) (▬▬▬) when $r_0 = 0.715$; laboratory data (○), analytical formula (3) (——), and semi-analytical formula (4) (▬▬) when $r_0 = 0.43$.

in a 0.07 m-deep uniform flow are presented in Fig. 2. The squares and circles denote the experimental results when piers were arranged in one row and in two rows, respectively. The thin dotted line and the thin solid line represent the results obtained by applying the analytical formula (3) for one-row ($r_0 = 0.715$) and two-row cases ($r_0 = 0.43$), respectively. The thick dotted line and the thick solid line represent the results obtained by applying the semi-analytical formula (4) for one-row and two-row cases, respectively. The formulas were evaluated using $n_b = 0.012$ (smooth steel bottom), $C_D = 2.1$ (square pier), $b = 0.114$ m, $h = 0.07$ m, and $w = 28.6$ and 8.6 cm for one-row and two-row cases, respectively.

First, the experimental results were compared with the results of calculations using the analytical formula (3), which neglects the drag interaction effect and corresponds to Eq. (4) with $C_{\mathrm{DI}} = 1$. The thin dotted line representing the one-row case ($r_0 = 0.715$) agrees with the data observed in experiments with sufficient longitudinal space, i.e. approximately $s/b > 4$, while the line disagrees with the data within $s/b < 4$. From this comparison, it can be inferred that when $s/b > 4$, the data is not influenced by the drag interactions of piers in the longitudinal direction, but when $s/b < 4$, the data is influenced by drag interactions. It can also be inferred that when $r_0 = 0.715$, the data was not influenced by the drag interactions of piers in the transverse direction. This agrees with the assumption that when $r_0 > 0.643$ (for square piers), $C_{\mathrm{DIT}} = 1$ (see Eqs. (7) and (9)). The thin solid line ($r_0 = 0.43$) is not consistent with the data observed over the entire range for the two-row case because of the transverse and longitudinal drag interaction effects of the piers.

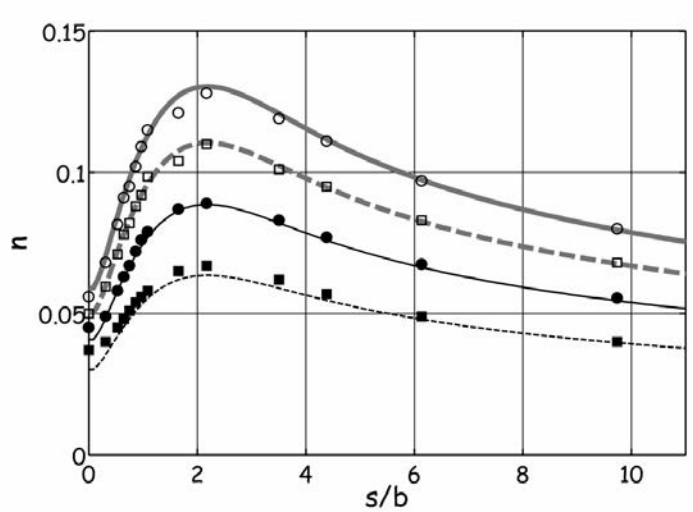

Fig. 3. Variation of the n values according to s/b when $r_0 = 0.43$. Laboratory data (○) and semi-analytical formula (——) when $h = 9$ cm; laboratory data (□) and semi-analytical formula (– – – –) when $h = 7$ cm; laboratory data (●) and semi-analytical formula (——) when $h = 5$ cm; laboratory data (■) and semi-analytical formula (– – – –) when $h = 3$ cm.

Next, the experimental results were compared with the results of calculations using the semi-analytical formula (4), which includes the drag interaction effects by incorporating the longitudinal drag interaction coefficient C_{DIF} in Eq. (6) and the transverse drag interaction coefficient C_{DIT} in Eq. (7). The thick dotted line representing the one-row case ($r_0 = 0.715$) indicates the results obtained by applying the semi-analytical formula (4) with Eq. (6) for C_{DIF} and $C_{\mathrm{DIT}} = 1$. The thick solid line representing the two-row case ($r_0 = 0.43$) indicates the results of applying the semi-analytical formula (4) with Eq. (6) for C_{DIF} and $C_{\mathrm{DIT}} = 3.08$. The value 3.08 for the transverse drag interaction coefficient C_{DIT} was evaluated by using Eq. (7) with $r_0 = 0.43$. For both one-row and two-row cases, the experimental data and the semi-analytical formula, including the drag interaction effect, agree well with each other.

The comparisons between experimental data and results derived using the semi-analytical formula (4), for various water depths, are shown in Fig. 3. The symbols represent experimental data obtained by using two rows ($r_0 = 0.43$) of square piers in 0.03, 0.05, 0.07, 0.09 m-deep uniform flows. The lines were obtained using the semi-analytical formula (4) with $n_b = 0.012$ (smooth steel bottom), $C_D = 2.1$ (square pier), $b = 0.114$ m, $C_{\mathrm{DIT}} = 3.08$, and Eq. (6) for C_{DIF}. When the water depth was varied, the results obtained using the semi-analytical formula, including the effects of drag interaction, agreed well with the experimental data.

Based on the observed agreement, it can be said that the empirical coefficients C_{DIF} and C_{DIT} are valid under the experimental conditions and that the longitudinal drag interaction coefficient C_{DIF} strongly depends on the longitudinal interval per

unit pier width (s/b) regardless of the change in porosity (r_0) or the water depth (h). Even though two (one-row and two-row) different cases were not sufficient to verify formula (7) for C_{DIT}, it is expected that the transverse drag interaction coefficient C_{DIT} strongly depends on porosity (r_0) regardless of the change in the longitudinal intervals (s/b) or the water depth (h). Note that in order to verify formula (7) for the transverse drag interaction coefficient C_{DIT}, we performed three-dimensional simulations with various porosities. The results are presented later in this paper.

The experimental data and the results derived using the semi-analytical formula for n suggest the following. For $s/b < 4$ (i.e. for an insufficient longitudinal space), the resistance of upstream piers affects the resistance of downstream piers, since the approach velocity decreases due to the turbulent eddies. At $s/b \approx 2.2$, the n value reaches its maximum. For $s/b < 2.2$, the n value decreases as the longitudinal space between the piers is reduced. For $s/b > 2.2$, the n value decreases, because the number of piers per unit longitudinal length decreases. As shown in Eq. (4), the n value increases as porosity decreases.

In the absence of the drag effects of resistant bodies, the Manning's roughness coefficient (n_b) is almost independent of water depth as long as the ratio of bottom roughness height to water depth is small. And, when the resistant bodies are present, the Manning's roughness coefficient (n_b) due to bottom roughness is negligible and thus the n value is proportional to water depth to the 2/3 power, $h^{2/3}$ in Eq. (3) or (4). The relationship between water depth (h/b) and n is presented in Fig. 4. Figures 4(a) and 4(b) show the results using one-row and two-row cases, respectively. The symbols denote the experimental data and the lines denote the results calculated

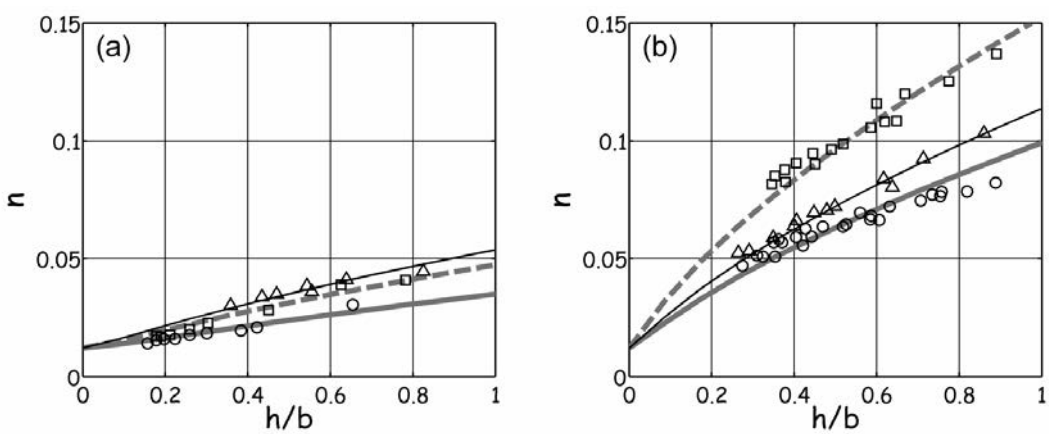

Fig. 4. Variation of the n values according to h/b. (a) One-row case ($r_0 = 0.715$): laboratory data (○) and semi-analytical formula (——) when $s/b = 0.316$, laboratory data (□) and semi-analytical formula (– – –) when $s/b = 0.754$, laboratory data (△) and semi-analytical formula (——) when $s/b = 4.386$; (b) two-row case ($r_0 = 0.43$): laboratory data (○) and semi-analytical formula (——) when $s/b = 0.535$, laboratory data (□) and semi-analytical formula (– – –) when $s/b = 2.175$, laboratory data (△) and semi-analytical formula (——) when $s/b = 6.14$.

using the semi-analytical formula (4). The experimental data and the semi-analytical formula show reasonable agreement. As the water depth increases, (i.e. the projection area of resistant piers increases), the n value increases. However, a larger number of additional experimental cases with deeper water depths are necessary in order to verify that the n value increases with water depth to the 2/3 power due to the unsubmerged piers, as reported previously. Three-dimensional simulations of these cases were performed and the results will be presented later in the next section.

4. Three-Dimensional Numerical Experiments

4.1. *Model setup*

For three-dimensional numerical experiments, the Reynolds Averaged Navier–Stokes (RANS) equation model of FLOW-3D, a computational fluid dynamics code, was employed. We chose the Generalized Minimal Residual Solver (GMRES) scheme for pressure-velocity coupling, and the first order upwind scheme for discretization of the momentum equation. The VOF model was chosen for free surface, the Fractional Areas/Volumes Obstacle Representation (FAVOR) was chosen for efficient geometry definition. And the standard $k-\varepsilon$ model with the standard wall function was chosen for the turbulence model. The constants required for the turbulent model followed its default values in the simulations presented in this study. A detailed description of the code and its theoretical background can be found in the FLOW-3D manual [Flow Science, Inc., 2000]. The results of numerical experiments were compared with observed experimental data prior to investigation, in order to validate the performance of the code in the experimental conditions.

To model square piers that are aligned in rows, the computational domain was assumed to include half of a 11.4 cm-wide square pier as shown in Fig. 5(a). Symmetry boundaries and periodic boundaries were chosen as shown in Fig. 5(b). For upstream and downstream boundaries, the periodic boundary condition, which interconnects data such as velocity components and water fractions between the two boundaries, was set to model infinite numbers of piers in the longitudinal direction and to achieve a fully developed and uniform flow as in an infinitely long channel. For lateral boundaries, the symmetry boundary condition was set to model infinite numbers of rows in the transverse direction. The smooth wall (no-slip) condition was set for the bottom boundary and the pressure outlet condition was set for the upper boundary. The channel slope of 0.0049 was set by increasing the x-component gravity. The water depth, which was less than the pier height, was determined by the initial water fraction. The computational grids were 0.0028 m in all directions. As in the laboratory experiment, the Reynolds number was maintained in the region $\mathrm{Re} > O(10^4)$ so that the drag coefficient of the square pier would remain constant. The n value was calculated by substituting the channel slope, the computed water depth, and discharge into the Manning's equation.

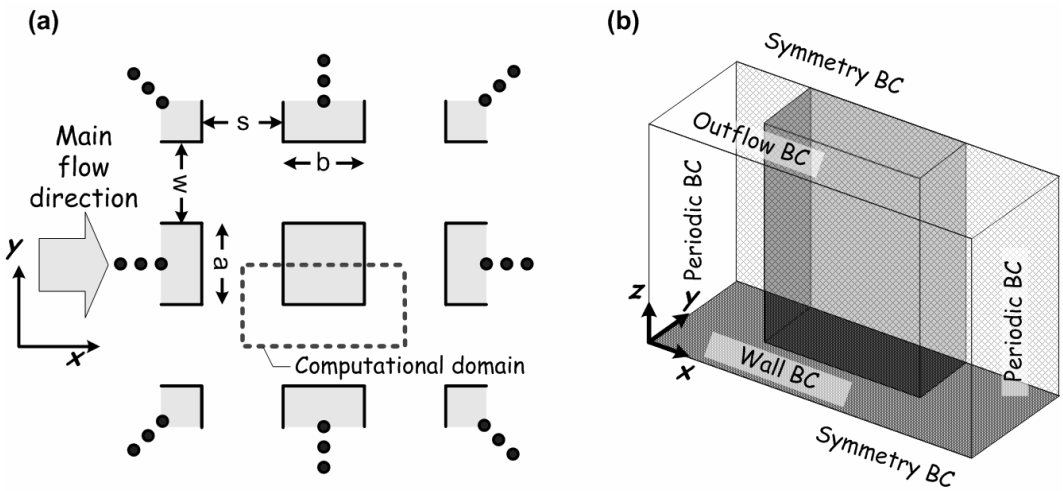

Fig. 5. Schematic diagrams of the numerical experiment. (a) Computational domain and (b) boundary conditions.

4.2. *Results*

For the purpose of validating the performance of the three-dimensional model, we simulated the two-row ($r_0 = 0.43$) case that was examined during the laboratory experiments, and compared the simulation results with the laboratory data. For this simulation, the longitudinal pier intervals were set in the range from 0.023 to 0.912 m with two uniform water depths, 0.05 and 0.09 m.

Figure 6 shows the distribution of n values for various longitudinal pier intervals (s/b) for both $h = 0.05$ m and $h = 0.09$ m. In this figure, the solid symbols denote the simulation data, the empty symbols denote the laboratory experimental data, and the lines denote the semi-analytical formula. The formula used to calculate n was evaluated by assuming values of $n_b = 0.012$ (smooth steel bottom), $C_D = 2.1$ (square pier), $b = 0.114$ m, $r_0 = 0.43$, $h = 0.05$ or 0.09 m, and the formulas of C_{DIF} in Eq. (6) and C_{DIT} in Eq. (7). The results of the three different approaches agreed well with each other, which implies that all three are reliable, and by extension that the results of the three-dimensional numerical simulations are reasonable, at least under the present experimental conditions.

In the previous section, investigations of the relationship between the equivalent resistance coefficient and the longitudinal pier interval in cases with porosity $r_0 = 0.715$ and 0.43 were presented. Using the three-dimensional numerical model, the additional cases with porosity $r_0 = 0.55$ and 0.3 (with $h = 0.09$ m) were simulated for various longitudinal pier intervals ($s/b = 0.2 \sim 8.0$) and the results were compared in Fig. 7 with those derived using the semi-analytical formula (4). The porosities ($r_0 = 0.55$ and 0.3) of the cases are smaller than 0.643 (see Eqs. (7) and (9)), and in these cases, the transverse drag interactions affect the total flow resistance.

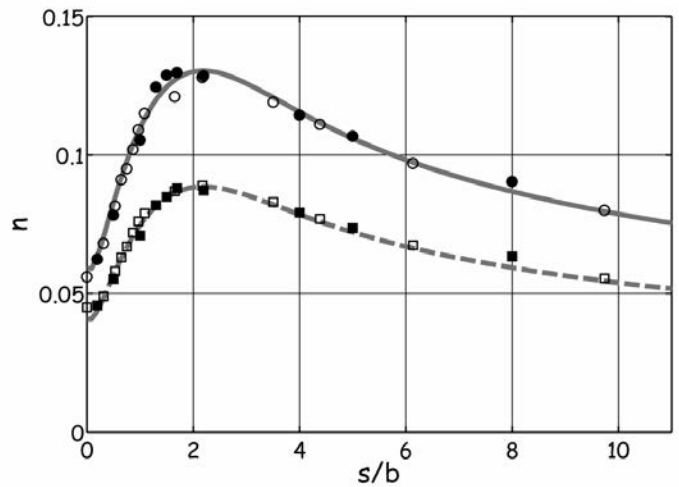

Fig. 6. Variation of the n values according to s/b when $r_0 = 0.43$. Laboratory data (□), numerical data (■), semi-analytical formula (▬▬▬) when $h = 0.05$ m; laboratory data (○), numerical data (●), semi-analytical formula (▬▬▬) when $h = 0.09$ m.

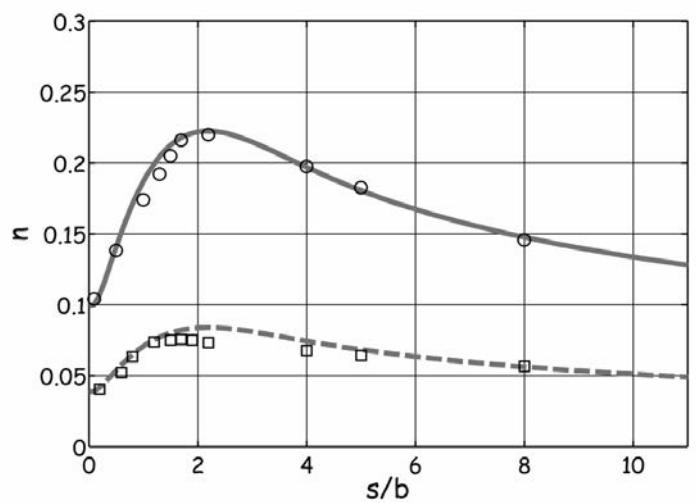

Fig. 7. Variation of the n values according to s/b when $h = 0.09$ m. Numerical data (○), semi-analytical formula (▬▬▬) when $r_0 = 0.3$; numerical data (□), semi-analytical formula (▬▬▬) when $r_0 = 0.55$.

In Fig. 7, the symbols denote the results of numerical experiments, and the lines denote the n values obtained using the semi-analytical formula (4). The results show good agreement in each case, which confirms that the relationship between the equivalent resistance coefficient and the longitudinal pier interval assumed by the semi-analytical n formula (4) is reasonable. In other words, the empirical formula (6) for the longitudinal drag interaction coefficient is found to be valid in various porosity

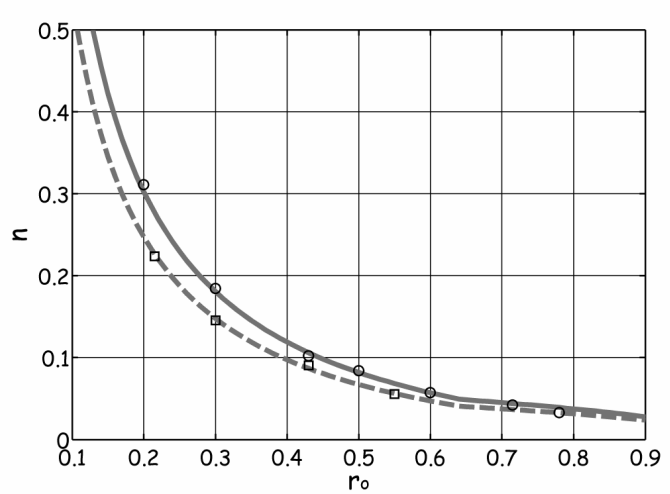

Fig. 8. Variation of the n values according to r_0 when $h = 0.09$ m. Numerical data (○), semi-analytical formula (——) when $s/b = 5.0$; numerical data (□), semi-analytical formula (– – –) when $s/b = 8.0$.

cases. The agreement also indicates that the relationship between the equivalent resistance coefficient and porosity r_0 assumed by the semi-analytical n formula (4) is reasonable. In other words, the transverse drag interaction coefficient (7), which is based on the orifice energy loss coefficient in the range $r_0 < 0.643$, was found to be valid for various longitudinal intervals.

Since the orifice energy loss coefficient increases as porosity decreases, the effect of the transverse drag interaction becomes stronger and the equivalent resistance coefficient becomes larger as the transverse interval space decreases. To illustrate this variation, the variation in the equivalent resistance coefficient according to porosity (transverse pier interval per unit channel width) is presented in the following figures.

Figure 8 represents the change in n for various porosities in cases with $s/b = 5.0$ and 8.0, in which the longitudinal drag interaction can be neglected (i.e. $C_{\mathrm{DIF}} = 1$) because $s/b > 4.0$, as mentioned earlier. The water depth was 0.09 m. The symbols denote the data derived from the numerical experiment and the lines denote calculations using the semi-analytical n formula. There is a discontinuity on the line of the semi-analytical formula because the transverse drag interaction coefficient C_{DIT} was evaluated using Eq. (7) when $r_0 < 0.643$ and $C_{\mathrm{DIT}} = 1$ when $r_0 > 0.643$. Within the range in which the longitudinal drag interaction can be neglected (i.e. $s/b > 4.0$), the results of numerical simulation agree well with the values of n derived using the semi-analytical formula (4) including the transverse drag interaction coefficient. Thus, it can be said that the transverse drag interaction coefficient, which was derived based on the orifice energy loss coefficient, is valid in this experimental range. In the figure, it can be seen that the n value decreases as the porosity in the transverse direction increases, because the orifice energy loss coefficient decreases as the porosity increases.

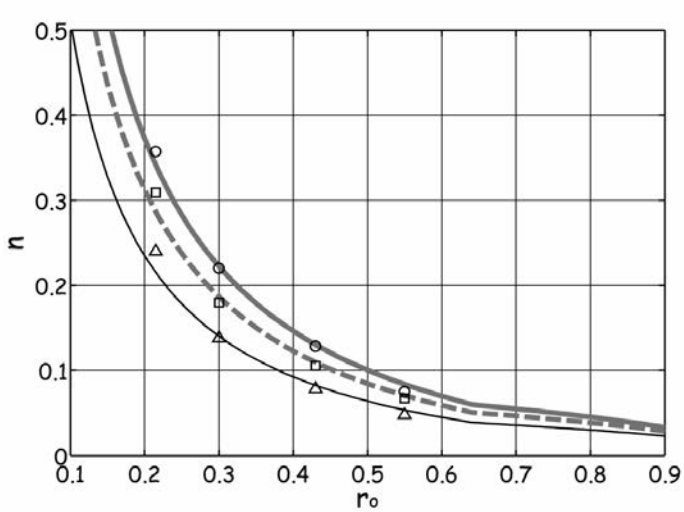

Fig. 9. Variation of the n values according to r_0 when $h = 0.09$ m. Numerical data (○), semi-analytical formula (——) when $s/b = 2.2$; numerical data (□), semi-analytical formula (– – – –) when $s/b = 1.0$; numerical data (△), semi-analytical formula (———) when $s/b = 0.5$.

Figure 9 represents the values of n for various porosities ($0.215 \sim 0.55$) in cases with $s/b = 2.2$, 1.0, and 0.5, in which the longitudinal drag interaction cannot be neglected because $s/b < 4.0$. The water depth was 0.09 m. The symbols denote the results of numerical experiments and the lines denote the results derived using the semi-analytical formula. To calculate n using the semi-analytical formula, the transverse drag interaction coefficient C_{DIT} was evaluated using Eq. (7) when $r_0 < 0.643$ and $C_{\mathrm{DIT}} = 1$ when $r_0 > 0.643$ as mentioned earlier. The numerical results are in good agreement with n derived using the semi-analytical formula (4) including the transverse drag interaction coefficient. The transverse drag interaction coefficient is also valid in the range when the longitudinal drag interaction cannot be neglected (i.e. $s/b < 4.0$).

In the previous section, we presented the n values according to water depth (h/b) observed during the laboratory experiments. However, as mentioned above, experiments with larger water depth are needed for verification of the relationship between the n value and water depth in Eq. (4). Due to limitations in the laboratory facilities, three-dimensional numerical experiments were performed for conditions in which the drags of the unsubmerged piers interact with each other at deeper water depths than those observed in the laboratory experiments. The porosity was $r_0 = 0.43$, the longitudinal pier intervals were $s/b = 0.754$, 2.175, and 4.386, and the water depths ranged from 0.0285 to 0.342 m. Figure 10 shows numerical results (filled symbols), laboratory observations (empty symbols), and the semi-analytical approaches (lines). The semi-analytical results were obtained using Eq. (4) with $C_{\mathrm{DIT}} = 3.08$ from Eq. (7) and $C_{\mathrm{DIF}} = 0.25$, 0.80, 1.0 from Eq. (6) with $s/b = 0.754$, 2.175, and 4.386, respectively. It can be said that when $s/b = 0.754$ and

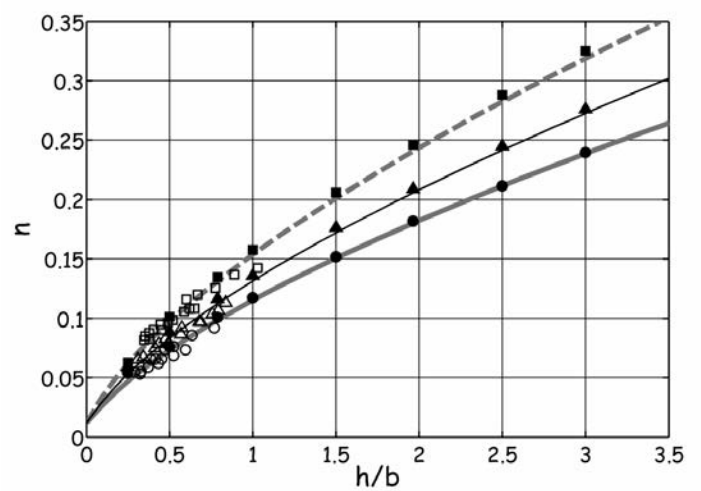

Fig. 10. Variation of the n value according to the water depth h/b when $r_0 = 0.43$. Laboratory data (○), numerical data (●) and semi-analytical formula (——) when $s/b = 0.754$; laboratory data (□), numerical data (■), and semi-analytical formula (– – – –) when $s/b = 2.175$; laboratory data (△), numerical data (▲), and semi-analytical formula (——) when $s/b = 4.386$.

2.175 both transverse and longitudinal drag interactions are involved, while when $s/b = 4.386$ only transverse drag interaction is involved. As shown, the results of the three different approaches agreed with each other. The simulations and the semi-analytical results show good agreement for water depths deeper than the laboratory setup would allow. This agreement confirmed that when unsubmerged square piers are aligned in rows in fully developed turbulent open channel flow, the equivalent resistance coefficient n is proportional to the 2/3 power of water depth as shown by the semi-analytical formula (4).

5. Application: Simulation of Tsunami Inundation

The most destructive tsunami in the history of Korea was the 1983 Tsunami. It was generated by an M 7.7 earthquake off Akita coast of Japan. This tsunami struck the east coast of Korea and caused two casualties and a considerable amount of property damage to Imwon Harbor (Fig. 11). We simulated the 1983 tsunami inundation at Imwon Harbor to test the application of the equivalent resistance coefficient by comparing the simulation results and observed data.

To apply the equivalent resistance coefficient to the inundation simulation, we chose the semi-analytical formula (10), which is a function of plane porosity R_0, instead of the formula (4). Note that Eq. (10) is equal to Eq. (4) if the transverse interval (w) is the same as the longitudinal interval (s) of the square piers as mentioned earlier. We chose this formula because estimating R_0 is easier than estimating w and s for randomly distributed buildings in the built-up area.

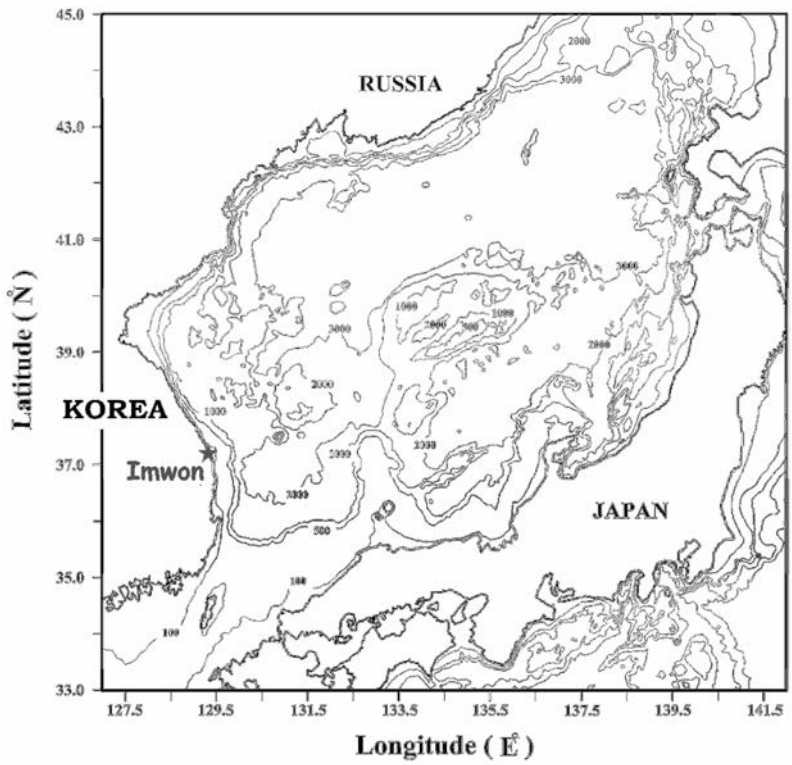

Fig. 11. Full tsunami simulation domain and location of Imwon (pentagram) Harbor in Korea.

Aburaya and Imamura [2002] proposed an equivalent roughness coefficient formula, which depends on the building occupancy ratio (i.e. $1 - R_0$), for modeling tsunami inundation. Their formula is the same as Eq. (4) except for the drag interaction coefficient, C_{DI}. As described earlier, Aburaya and Imamura [2002] mentioned that their drag coefficient should be a function of shapes and alignments of houses and unsteadiness of the flow. And to investigate the drag interaction effect, they performed an experimental result using longitudinally aligned piers. However, they did not propose a general expression for drag interaction effect, and Koshimura *et al.* [2009] did not take into account the drag interaction effect among the buildings, i.e. $C_{\mathrm{DI}} = 1$ in the tsunami simulation. As a result, compared with the present formula (10), their formula does not take into account the transverse drag interaction, thus, it does not properly estimate the drag interaction varied according to the building occupancy ratio.

To see the effect of drag interaction, the variation of the equivalent roughness coefficient according to the plane porosity R_0 is presented in Fig. 12. In the figure, the present formula is compared with the formula excluding drag interaction (i.e. $C_{\mathrm{DI}} = 1$) when $h = 2.0$ m and $b = 4.0$ m; $h = 1.0$ m and $b = 4.0$ m; and $h = 1.0$ m and $b = 8.0$ m as shown in panel (a) panel (b) and panel (c), respectively. From the

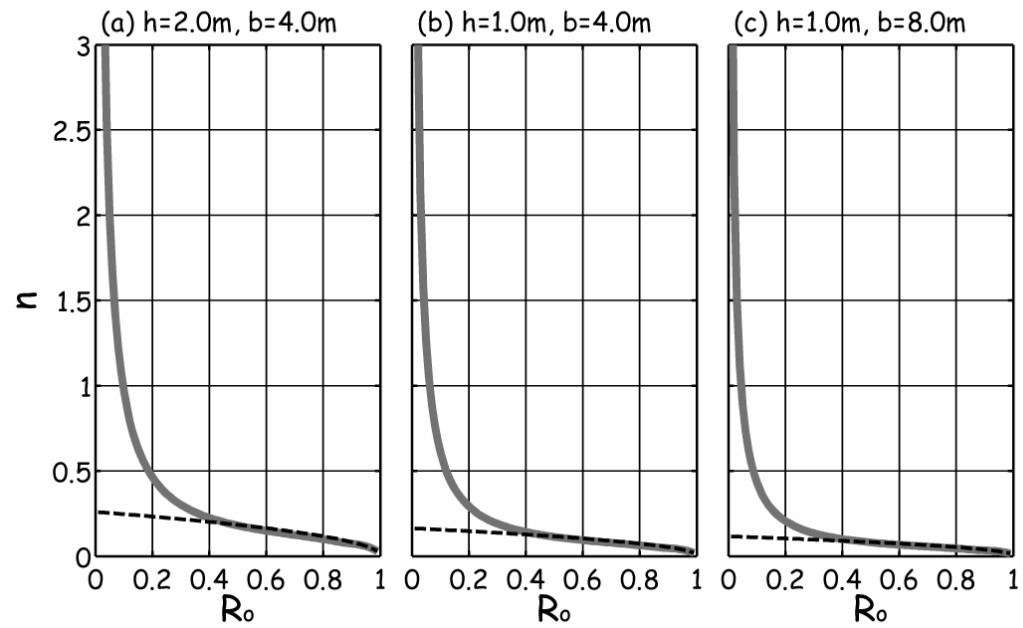

Fig. 12. Variation of the n values according to the plane porosity R_0. (a) $h = 2.0$ m and $b = 4.0$ m; (b) $h = 1.0$ m and $b = 4.0$ m; (c) $h = 1.0$ m and $b = 8.0$ m. The present formula in Eq. (10) (——) and the formula excluding drag interaction (i.e. $C_{\mathrm{DI}} = 1.0$) (– – – –).

figure, it was found that as the plane porosity decreases (i.e. the building occupancy ratio increases), the equivalent roughness coefficient increases. Differently from the n formula excluding drag interaction, the present semi-analytical n formula rapidly increases when $R_0 < 0.3 \sim 0.4$

Prior to presenting the simulation, it should be mentioned that the semi-analytical formulas (4) and (10) are valid only if the buildings are square, unsubmerged, and arranged at equal intervals and the main turbulent flood flow runs perpendicular to the aligned buildings. We also assumed that flow was locally uniform and stationary. Therefore, the validity of its application to inundation simulations for built-up areas, in which buildings are randomly distributed and sized, is beyond the scope of the assumptions in this study. However, an approach using the equivalent resistance coefficient formula may offer a good and efficient approximation of the built-up area as it takes into account the effects of drag interactions and drag that increases with water depth.

For the inundation simulation, we utilized a previously published nonlinear shallow-water equation model [Lim *et al.*, 2008] and applied the semi-analytical formula (10) to this model. As mentioned earlier in this paper, an approach using the equivalent resistance coefficient that neglects the buildings in the relatively coarse grid system is more practical and efficient for inundation simulation over built-up areas than an approach using a fine grid system that resolves each building. The

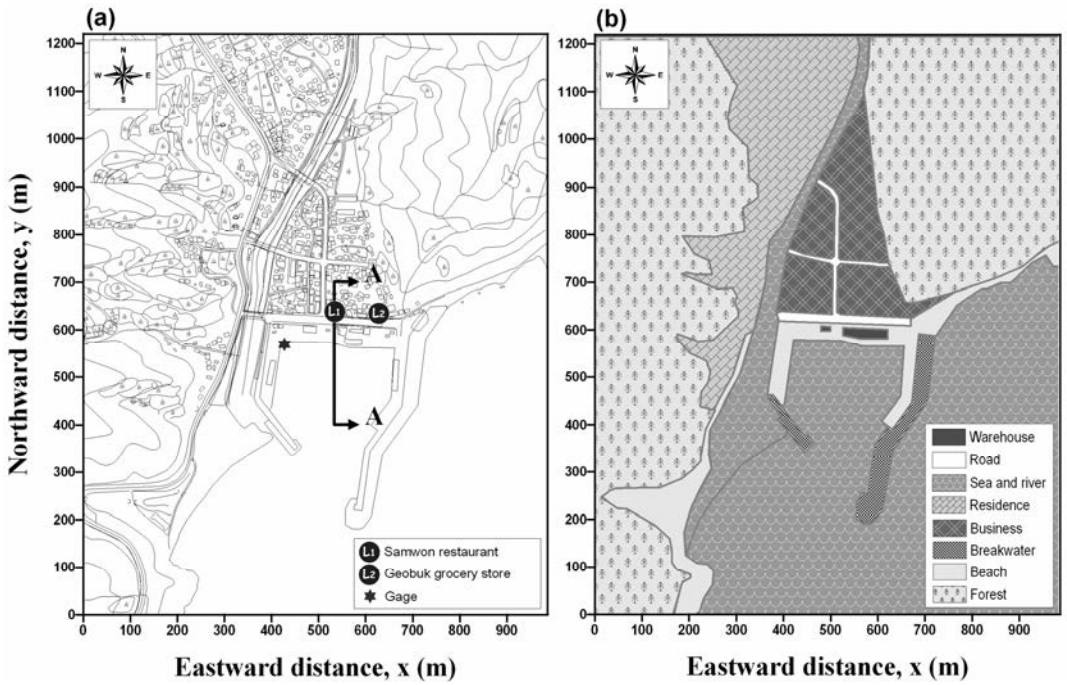

Fig. 13. Map of Imwon Harbor. (a) Built-up area and its surroundings for computational domain with finest grids and (b) areas characterized by their resistant environments.

equivalent resistance coefficient approach was expected to be more accurate than a conventional approach assuming a constant n that excludes the drag effects of the buildings. The inundation simulation results were compared with the results of the other simulation assuming $n = 0.025$ and the run-up heights observed at locations L_1 and L_2 as shown in Fig. 13(a).

5.1. *Model setup*

For the tsunami simulation, we combined a linear Boussinesq-type wave equation model with a dispersion-correction technique [Yoon *et al.*, 2007] and a nonlinear shallow-water equation model [Lim *et al.*, 2008] with a moving boundary technique [Yoon and Cho, 2001]. The linear Boussinesq-type wave equation was used to model far-field tsunami propagation simulation in the region where wave dispersion is significant. The nonlinear shallow-water equation was used to simulate near-field tsunami propagation and inundation in the region where nonlinear effects and energy dissipation of waves are dominant.

Lim *et al.* [2008] provide details of numerical schemes, initial and boundary conditions and bathymetry used in the present propagation simulation of the 1983 Tsunami over the East Sea. For the tsunami simulation using five-step grid refinement, finer grid system was nested dynamically into the next coarser grid system

which has three times a larger grid size. The finest grid system with 4.5 m grid size resolves Imwon Harbor, and the coarsest grid region includes the East Sea. For the inundation simulation, the finest grid region was constructed to include the built-up area with omitting the buildings in Imwon. The time step for the finer grid region was also 1/3 of that for the coarser grid region, but the time step size for the final three finest grid regions was chosen equally to reduce numerical diffusion errors caused by the upwind technique. The time step for the coarsest grid region was 3.0 s while that for the finest grid region was 0.11 s.

In order to apply the equivalent resistance coefficient to the built-up area shown in Fig. 13(a), the computational domain was divided into business, residence, road, sea, river, beach, breakwater, warehouse, and forest areas as presented in Fig. 13(b). The x (eastward distance) and y (northward distance) coordinates presented in Fig. 13 were taken in order to demonstrate locations in Imwon Harbor and its surroundings. The semi-analytical formula (10) was employed for the residence and business areas, while for the other areas the empirical constant n values were chosen based on Chow [1959]. The constant n value (i.e. $n = n_b$) was set to 0.025 for sea, beach, river, and road areas, 0.04 for breakwater area, and 0.08 for forest area. Since roads in the built-up area play a role in waterway during inundations, the main roads in the business area was characterized by a constant n value. For the residence and warehouse areas, the n value was evaluated by using formula (10), where we used $n_b = 0.025$, $R_0 = 40\%$, $b = 4$ m, and $C_D = 2.1$. For the business area, the n value was also evaluated with $n_b = 0.025$, $R_0 = 7\%$, $b = 4$ m, and $C_D = 2.1$. The values of the drag interaction coefficient were obtained with Eqs. (6) and (7) which can be rewritten as a function of the plane porosity R_0. The total water depth h can be obtained by solving the shallow-water equation at each grid point. For the built-up area with randomly distributed and sized buildings, the plane porosity R_0 was roughly estimated from the densest block in each area and the representative building width b was estimated from the smallest building in the densest block. For the comparison purpose, an additional inundation simulation with a constant n value of 0.025 (a conventional value for flood areas) over the whole inundation area was conducted.

5.2. *Results*

A simulated time series of water surface elevations at a gage grid point is presented in Fig. 14. The gage grid point represented by a hexagram symbol in Fig. 13(a) is located at the upper-left corner of the harbor. The first tsunami reached Imwon Harbor 113 min after its generation and the maximum tsunami elevation was 4.5 m, after 155 min. At this location, the results of the present simulation and the conventional simulation using $n = 0.025$ are the same.

Figure 15 shows the distributions of maximum water surface elevation obtained from the present simulation (Fig. 15(a)) and the simulation using $n = 0.025$

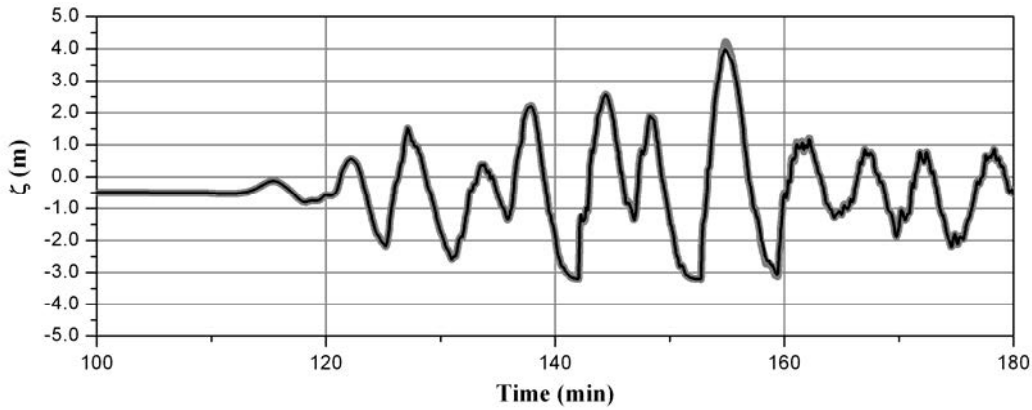

Fig. 14. Time series of the water surface elevation above MSL at a gage grid point in Imwon Harbor. Present simulation (▬▬) and simulation with $n = 0.025$ (——).

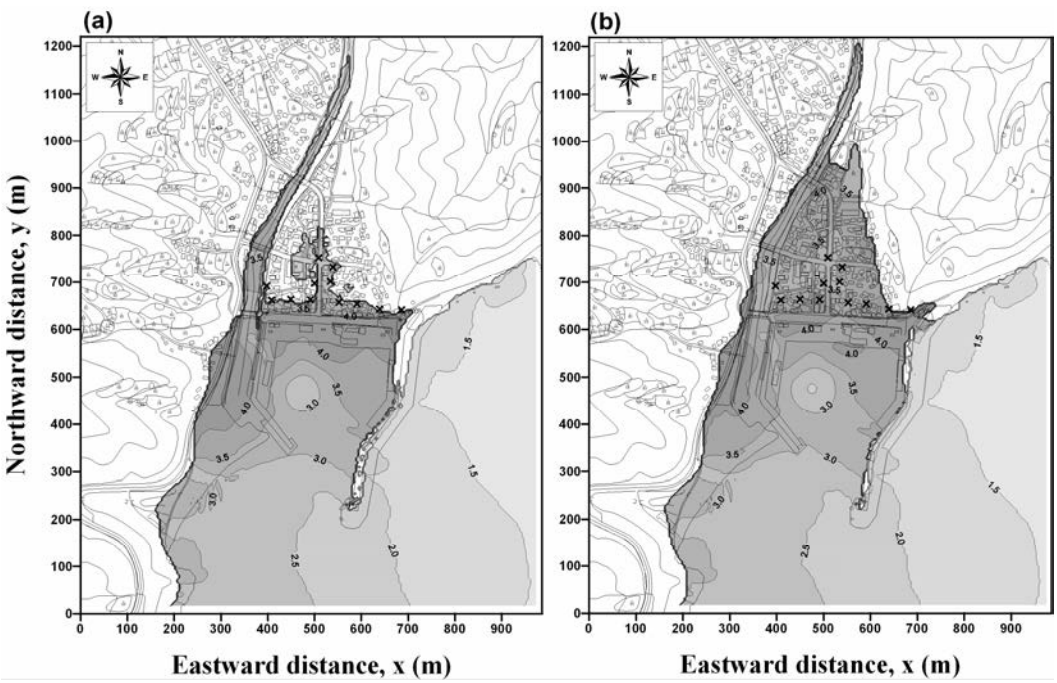

Fig. 15. Observed inundation boundary (×) and distribution of the maximum water surface elevation above MSL (unit: m). (a) Present simulation; (b) simulation with $n = 0.025$.

(Fig. 15(b)). In the seawater region shown in Figs. 15(a) and 15(b), the distributions of the two simulations are similar to each other. The inundation regions of the two simulations, however, show a significant difference. The inundation area calculated with the present equivalent n value is limited by the blocking effect due to front buildings and agrees well with the observed inundation boundary presented

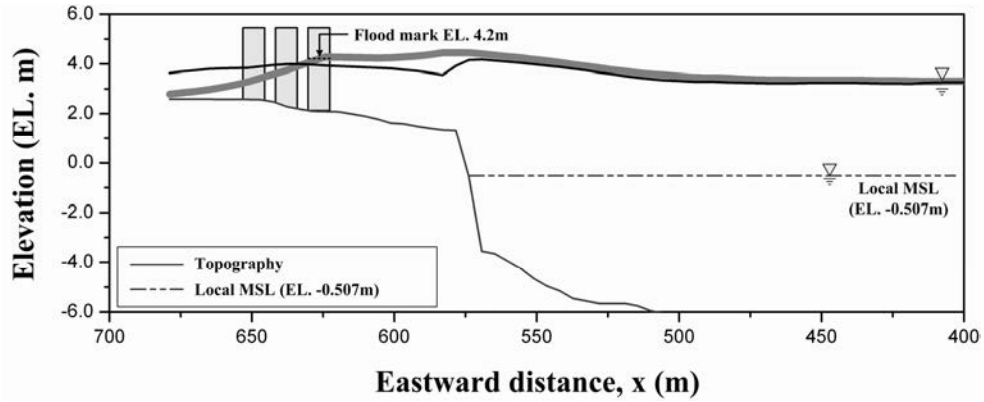

Fig. 16. Profiles of the maximum water surface elevation along a cross-section at $x = 530$ m. Present simulation (——) and simulation with $n = 0.025$ (——).

by cross symbols in Fig. 15. On the other hand, the conventional simulation with a constant n value gives a complete inundation over the whole business area.

Figure 16 shows the cross-sectional profiles of maximum inundation elevation. The profile obtained from the present simulation using equivalent n value shows the blockage effect due to drags of the front buildings, but the other profile calculated using the constant n value does not show this effect. The result representing the blockage effects due to buildings are similar to the result of investigation using emergent vegetation presented in Yanagisawa *et al.* [2009].

Figure 17 presents a simulated time series of water surface elevations at the location of Samwon restaurant (shown in Fig. 15). The maximum water surface elevation reached at the location around 155 min after the generation. The minimum elevation 2.0 m in the time series represents the ground level at the location. At this

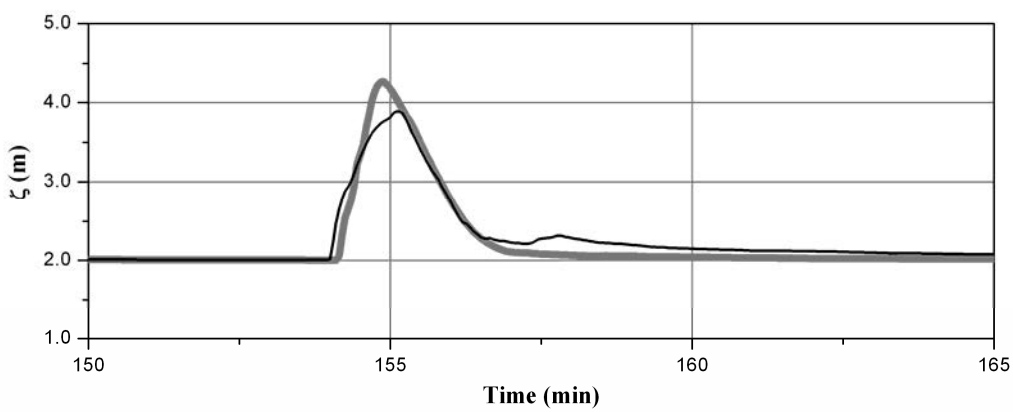

Fig. 17. Time series of the water surface elevation above MSL at the location of Samwon restaurant (presented by L_1 in Fig. 11). Present simulation (——) and simulation with $n = 0.025$ (——).

Table 1. Observed and computed run-up heights above MSL.

	Location	Observation	Computation with the constant n value	Computation with the equivalent n value
L_1	Samwon restaurant	4.20 m	4.04 m	4.26 m
L_2	Geobuk grocery store	4.30 m	4.12 m	4.41 m

location, the result of the present simulation is larger than that of the conventional simulation using $n = 0.025$ because of the blockage effect due to drags of the front buildings.

Table 1 indicates a comparison among the observed run-up heights and the results of the present simulation and the simulation using the constant n value (i.e. $n = 0.025$). The locations of run-up observation points L_1 and L_2 are presented in Fig. 13(a). The results obtained using the equivalent resistance coefficient are within the range of approximately $4.2 \sim 4.4$ m at the observation locations and are close to the observed run-up heights.

6. Conclusion

The equivalent resistance coefficient (n) was investigated and applied to inundation simulations over a built-up area using a relatively coarse grid system. To investigate the n value, a semi-analytical formula was derived from momentum analysis including drag and drag interaction effects being evaluated, assuming square unsubmerged rigid piers aligned in rows. Both laboratory and numerical experiments were conducted for aligned piers in open channel turbulent flows. From the comparisons between the results derived using the semi-analytical formula and from the experiments, we found that the n value is strongly dependent on the intervals between the piers, and elucidated the relationships between n and hydraulic characteristics such as water depth and intervals between piers. When the longitudinal interval space becomes narrower than four times the pier width, drag interaction plays a role in decreasing the total resistance in comparison with the case of sparse arrangement. As the longitudinal interval space becomes narrower than 2.2 times the pier width, the n value decreases because of the longitudinal drag interaction. As the longitudinal interval space becomes wider than 2.2 times the pier width, the n value decreases also because the pier number per unit channel length decreases. As the transverse interval space decreases, the n value increases because the pier number per unit channel width increases and the drag interaction increases the resistance, analogous to the orifice energy loss mechanism. We confirmed that the equivalent resistance coefficient n increased with water depth to the 2/3 power. Consequently, the proposed n formula was found to be accurate under the present experimental conditions.

In addition, the 1983 Tsunami inundation at Imwon Harbor was simulated using the n formula proposed in this study and the results were compared with the results

of simulation using a constant n value as well as reported inundation heights. The inundation flow simulated using the proposed n formula encountered more resistance increased with inundation water depth over the built-up area in Imwon than that derived through the simulation using a constant n value. We found that the results of the present simulation were more realistic and in better agreement with the reported inundation heights than the simulation results using a constant n value.

Since the proposed n formula is valid only if the square unsubmerged buildings are spaced at equal intervals and the main turbulent flood flow runs perpendicular to the aligned buildings, extended investigations of the equivalent resistance coefficient, which includes the drag interaction effects exerted by various arrangements and shapes of buildings, must be conducted.

Acknowledgments

This research was supported in part by a grant from the "Countermeasure System against Typhoons and Tsunamis in Harbor Zones" Program of the Ministry of Land, Transport and Maritime Affairs, Korea, and also from the Korea Meteorological Administration Research and Development Program under Grant CATER 2011-5209.

References

Aburaya, T. & Imamura, F. [2002] "The proposal of a tsunami runup simulation using combined equivalent roughness," *Ann. J. Coast. Eng.* **49**, 276–280 (in Japanese).

Bae, J. S., Choi, J. & Yoon, S. B. [2010] "Numerical simulation of tsunami inundation using equivalent resistance coefficient," *Proc. 17th Int. Association of Hydro-Environment Engineering and Research*, Asia and Pacific Division, New Zealand.

Chiew, Y. & Tan, S. [1992] "Frictional resistance of overland flow on tropical turfed slope," *J. Hydraul. Eng.* **118**, 92–97.

Choi, J., Ko, K. O. & Yoon, S. B. [2009] "3D numerical simulation for equivalent resistance coefficient for flooded built-up areas," *Proc. 5th Int. Conf. Asian and Pacific Coasts*, Singapore.

Choi, J., Kwon, K. K., Ko, K. O. & Yoon, S. B. [2009] "Hydraulic experiment for equivalent resistance coefficient for inundation simulation model," *Proc. 5th Int. Conf. Asian and Pacific Coasts*, Singapore.

Chow, V. T. [1959] *Open Channel Hydraulics* (McGraw-Hill Book Co., New York), pp. 97–114.

Flow Science, Inc. [2000] FLOW-3D User Manual.

Koshimura, S., Oie, T., Yanagisawa, H. & Imamura, F. [2009] "Developing fragility functions for tsunami damage estimation using numerical model and post-tsunami data from Banda Aceh, Indonesia," *Coast. Eng. J.* **51**(3), 243–273.

Kwon, K. K., Choi, J. & Yoon, S. B. [2010] "Estimation of equivalent resistance coefficient for uniform arrays of unsubmerged rigid obstructions," *Proc. 17th Int. Association of Hydro-Environment Engineering and Research*, Asia and Pacific Division, New Zealand.

Lim, C. H., Bae, J. S., Lee, J. I. & Yoon, S. B. [2008] "Propagation characteristics of historical tsunamis that attacked the east coast of Korea," *Nat. Hazards* **47**, 95–118.

Mei, C. C. [1989] *The Applied Dynamic of Ocean Surface Waves* (World-Scientific, Singapore) (2nd printing with correction).

Musleh, F. A. & Cruise, J. F. [2006] "Functional relationships of resistance in wide flood plains with rigid unsubmerged vegetation," *J. Hydraul. Eng.* **132**, 163–171.

Naot, D., Nezu, I. & Nakagawa, H. [1996] "Hydrodynamic behavior of partly vegetated open channels," *J. Hydraul. Eng.* **122**(11), 625–633.

Petryk, S. & Bosmajian, G. [1975] "Analysis of flow through vegetation," *J. Hydraul. Eng.* **101**, 871–884.

Struve, J., Falconer, R. A. & Wu, Y. [2003] "Influence of model mangrove trees on the hydrodynamics in a flume," *Estuarine Coast. Shelf Sci.* **58**, 163–171.

Teh, S. Y., Koh, H. L., Liu, P. L.-F., Ismail, A. I. M. & Lee, H. L. [2009] "Analytical and numerical simulation of tsunami mitigation by mangroves in Penang, Malaysia," *J. Asian Earth Sci.* **36**, 38–46.

Yanagisawa, H., Koshimura, S., Goto, K., Miyagi, T., Imamura, F., Ruangrassamee, A. & Tanavud, C. [2009] "The reduction effects of mangrove forest on a tsunami based on field surveys at Pakarang Cape, Thailand and numerical analysis," *Estuarine Coast. Shelf Sci.* **81**, 27–37.

Yoon, S. B. & Cho, J. H. [2001] "Numerical simulation of coastal inundation over discontinuous topography," *Water Eng. Res., Kor. Water Res. Assoc.* **2**(2), 75–87.

Yoon, S. B., Lee, J. I., Nam, D. H & Kim, S. H. [2006] "Energy loss coefficient of waves considering thickness of perforated wall," *J. Kor. Soc. Coast. Ocean Eng.* **18**(4), 321–328 (in Korean).

Yoon, S. B., Lim, C. H. & Choi, J. [2007] "Dispersion-correction finite difference model for simulation of transoceanic tsunamis," *Terr. Atmos. Ocean. Sci.* **18**(1), 31–53.